DOI: 10.1021/ma101218q

Macromolecules
ARTICLE

Hydrogen Adsorption by δ and ε Crystalline Phases of Syndiotactic Polystyrene Aerogels

Susana Figueroa-Gerstenmaier,*,§ Christophe Daniel,† Giuseppe Milano,† Jenny G. Vitillo,‡ Olena Zavorotynska,‡ Giuseppe Spoto,‡ and Gaetano Guerra*,†

†*Dipartimento di Chimica, NANOMATES and INSTM Research Unit, Università di Salerno, Fisciano (SA) 84084, Italy,* ‡*Dipartimento di Chimica IFM and NIS Centre of Excellence, Università di Torino, Via Giuria 7, Torino 10125, Italy, and* §*División de Ciencias e Ingenierías, Campus León, Universidad de Guanajuato, Loma del Bosque 103, León (Gto.) 37150, Mexico*

Received June 3, 2010; Revised Manuscript Received September 13, 2010

ABSTRACT: The H_2 uptake from s-PS samples exhibiting different crystalline phases and different morphologies has been studied by gravimetric measurements at 77 K in the hydrogen pressure range from 0 up to 1.7 MPa and compared with molecular simulations relative to s-PS crystals. Gravimetric experiments show that the molecular hydrogen sorption is strongly dependent on the sample morphology and is maximum for low-density polymer aerogels. However, independently of the morphology, the H_2 uptake is minimum for the dense β and γ crystalline phases, intermediate for the channel-shaped nanoporous ε phase, and maximum for the cavity-shaped nanoporous δ phase. In particular, although the two nanoporous crystalline phases present essentially the same density (0.98 g/cm^3), the hydrogen uptake from the δ phase is roughly double with respect to the uptake from the ε phase, both for powders and for aerogels. Infrared measurements and molecular simulations well agree with these quantitative sorption data and clearly indicate that, for both low and high pressure, the hydrogen molecules are preferentially adsorbed into the nanoporous crystalline phases. In particular, molecular simulations indicate that the maximum average hydrogen uptake is of nearly 3 molecules per cavity of the δ phase and of nearly 3.5 molecules per unit height of the channels of the ε phase.

Introduction

Nanoporous materials have been the focus of attention for solving the challenge of hydrogen storage in an efficient, cheap, and safe way. Among the most common materials considered to adsorb hydrogen[1] are porous carbons, nanotubes, zeolites, porous polymers, and metal−organic frameworks. There is a recent and excellent review[2] devoted to porous organic polymers where advantages, inconveniences, and applications are discussed for the different polymeric materials and where they are also compared with other types of materials. Different kinds of polymeric materials with very high surface areas, exhibiting irregular pores with a wide size distribution, have been obtained.

Recently, a new mechanism of H_2 uptake from polymeric materials based on adsorption in the ordered cavities of a nanoporous crystalline phase (the δ phase of syndiotactic polystyrene, s-PS), rather than on disordered amorphous surfaces, has been disclosed.[3]

s-PS is a semicrystalline stereoregular polymer (30−50% degree of crystallinity) which is easily crystallizable and high melting (ca. 270 °C) and presents a very complex polymorphic behavior. There are two crystalline phases with trans-planar chains (α and β) and three with helical s(2/1)2 chains (γ, δ, and ε).[4] Two of the helical crystalline phases (δ[5] and ε[6]) present nanopores, being able to absorb, even from diluted solutions, low-molecular-mass guest molecules in cavities of their crystalline structures,[7] eventually leading to the formation of host−guest cocrystalline phases.[8] The δ phase[5] presents two identical cavities and eight styrene monomeric units per unit cell, while the ε phase,[6] with 4 chains per unitary cell, exhibits channels parallel to the chain axes. It is worth noting that the sorption of gases (and in general of guest molecules) from polymer crystalline phases is a rather unusual phenomenon.

The two nanoporous crystalline phases of s-PS give us an ideal framework to explore and understand the adsorption mechanism of hydrogen inside polymeric materials where phenyl rings and microporosity are highly represented and spatially ordered. In this work, we present and compare the adsorption isotherms of hydrogen for δ and ε crystalline phases, as measured by gravimetric techniques and calculated by means of grand canonical Monte Carlo (GCMC) simulations.

The reported adsorption experiments refer to samples of different morphologies (films, powders, or aerogels[9] exhibiting different apparent densities) as well as presenting different nanoporous (δ and ε) or dense (β[10] or γ[11]) crystalline phases.

The hydrogen adsorption in samples exhibiting different crystalline phases has been also explored by FTIR spectroscopy at 20 K that, associated with the results of the GCMC simulations, contributes in understanding the basic mechanisms of interaction of the H_2 molecules within the crystalline cavities.

Experimental Section

Materials. s-PS was supplied by Dow Chemical under the trademark Questra 101. ^{13}C nuclear magnetic resonance characterization showed that the content of syndiotactic triads was over 98%. The weight-average molar mass obtained by gel permeation chromatography (GPC) in trichlorobenzene at 135 °C was found to be $M_w = 3.2 \times 10^5$ with the polydispersity index $M_w/M_n = 3.9$.

All s-PS gels were prepared in hermetically sealed test tubes by heating the mixtures above the boiling point of the solvent until complete dissolution of the polymer and the appearance of a transparent and homogeneous solution had occurred. Then the

*Corresponding authors: Tel +52 477 788 5100, Fax +52 477 788 5107, e-mail sfigueroa@fisica.ugto.mx (S.F.-G.); Tel +39 089 969558, Fax +39 089 969603, e-mail guerra@unisa.it (G.G.).

 Published on Web 09/30/2010

hot solution was cooled to room temperature where gelation occurred.

The δ aerogel samples were obtained by treating s-PS/toluene native gels with a SFX 200 supercritical carbon dioxide extractor (ISCO Inc.) using the following conditions: pressure = 200 bar, extraction time t = 60 min, T = 40 °C. The β aerogel samples were obtained by treating with the same apparatus s-PS/1,2-dichloroethane native gels using the following conditions: pressure = 200 bar, extraction time t = 120 min, T = 150 °C. As described in detail in ref 9d, ε aerogels were obtained by immersion in chloroform for 12 h of γ aerogels (obtained by supercritical carbon dioxide extraction at 130 °C of a sPS/1,2-dichloroethane gel) followed by chloroform extraction with supercritical carbon dioxide at the following conditions: pressure = 200 bar, extraction time t = 120 min, T = 40 °C.

The degree of crystallinity of the aerogels has been evaluated from X-ray diffraction data by applying the standard procedure of resolving the diffraction patterns into two areas corresponding to the contributions of the crystalline and amorphous fractions. For the aerogels considered in the present paper the degree of crystallinity is in the range 35−40%.

The porosity P of the aerogels can be expressed in function of their apparent density ρ as

$$P = 100\left(1 - \frac{\rho}{\rho_s}\right)$$

where ρ_s is the density of the polymer matrix (equal to 1.02 g/cm^3, for a semicrystalline δ-form s-PS sample with a crystallinity of nearly 40%). As described in detail in ref 9d, these aerogels present a fibrillar morphology with fibril diameters in the range 30−200 nm.

FTIR Measurements. For the transmission FTIR experiments, aerogels were used as prepared in form small cylinders with a diameter of about 1 and 0.5 cm thick. Before H_2 adsorption all the samples were outgassed overnight under high vacuum (residual pressure $< 10^{-6}$ bar) at 300 K to remove adsorbed impurities. This treatment was performed in the same cryogenic cell (a properly modified closed-circuit liquid helium Oxford CCC 1204 cryostat) allowing the infrared investigation of species adsorbed under controlled temperature (in the 300−14 K interval) and pressure (in the 0−0.5 bar interval) conditions. Typical IR experiments consisted of three steps: (i) 30 mbar of H_2 was initially dosed on the sample at 300 K. (ii) IR spectra were then recorded *in situ* while lowering the temperature down to 20 K. The samples were then left at this temperature in hydrogen for one night, allowing the aerogel−hydrogen system come to reach equilibrium conditions. (iii) IR spectra were finally recorded at fixed temperature (20 K) while stepwise outgassing hydrogen. For the sake of brevity, only the spectral series obtained for the β-, ε-, and δ-aerogels following step iii are shown here.

The infrared spectra were recorded on a Bruker Equinox 55 FTIR spectrometer (equipped with an MCT cryogenic detector) with the sample compartment modified to accommodate the cryogenic head; 256 interferograms (recorded at 1 cm^{-1} resolution) were typically averaged for each spectrum.

Sorption Isotherms. H_2 adsorption isotherms at 77 K were obtained by using ultrapure 6.0 grade H_2 (99.9999%V; SIAD) further purified before adsorption by diffusion through a Pd membrane based Johnson Matthey diffusion unit (H140/5). An intelligent gravimetric analyzer (IGA-002, supplied by Hiden Analytical Ltd., UK) was used, allowing to work in the 0−20 bar range and to get the 77 K temperature through the use of a liquid N_2 bath. This apparatus is an ultrahigh-vacuum system (UHV), which allows isotherms and the corresponding kinetics of adsorption and desorption to be determined, for set pressure steps. The mass uptake was measured as a function of time, and the approach to equilibrium of the mass relaxation curve was monitored in real time using a computer algorithm.

Buoyancy corrections were carried out using the weights and densities of all the components of the sample and counterweight sides of the balance and the measured temperature. The adsorbed mass m_a was calculated by the equation

$$m_a = \frac{\phi_s - \phi_u + \sum w_i \frac{\rho_{gi'} - \rho_{air}}{\rho_i - \rho_{air}} - \sum w_j \frac{\rho_{gj'} - \rho_{air}}{\rho_j - \rho_{air}} - m_s\left(1 - \frac{\rho_{gs'}}{\rho_s}\right)}{1 - \frac{\rho_{gs'}}{\rho_s}} \quad (1)$$

where ϕ_s is the balance reading after the gas adsorption, ϕ_u is the unload reading, m_s is the mass of the sample after the thermal treatment, w_i (ρ_i) and w_j (ρ_j) are the weights (densities) measured in air of the sample container and of the counterweight components, ρ_g is the density of the gas, ρ_s is the sample skeletal density, and ρ_{air} is the air density (1.1574 mg/cm^3). In this equation, the density of the gas ρ_g at the different points in the microbalance (counterweight, sample, and cabinet) was calculated by taking into account the different temperature at which these parts were. The density of the samples has been determined by helium isotherms conducted on the samples at 293 K in the 0−20 bar range. The isotherms obtained show absence of gas interaction phenomena. The helium adsorption/desorption scans have been repeated five times in order to verify the reproducibility of the measurement. This check was necessary because of the low density of the aerogel samples that makes fundamental the correction for the buoyancy, which can amount to up the 500% at 20 bar and 77 K in hydrogen. The linearity of the curve and the reproducibility of the scans indicate the absence of gas interaction, necessary for a correct evaluation of the sample volume. The skeletal volume of the sample was calculated from each curve by eq 1, assuming that no helium is adsorbed by the material (m_a = 0) and supposing that the decrease in the sample weight by increasing the pressure was due to only the Archimede's upthrust. ρ_s was obtained as m_s/V_s, where V_s is the average of the 10 values obtained for the skeletal volume .

The H_2 sorption from s-PS samples, as already described for the uptake of other guests (both gases and liquids),[5−7,9a,9c,9d] is reversible. In fact, essentially unaltered optical and sorption isotherms are obtained as a consequence of repeated H_2 sorption−desorption cycles. This is mainly due to the well-known structural stability of the nanoporous δ[5,7] and ε[6] nanoporous crystalline phases also in their aerogels.[9]

Molecular Simulations

We performed grand canonical Monte Carlo simulations to calculate the adsorption isotherms of hydrogen in the crystalline phases δ and ε of s-PS at 77 K. In this section, we explain first the procedure to simulate the adsorbents, following for the model information for the fluid, the cross-interactions, and the GCMC simulations details.

***δ* Crystalline Phase.** The monoclinic structure of the δ form of s-PS (a = 1.75 nm, b = 1.18 nm, c = 0.78 nm, γ = 118°, density = 0.977 g cm^{-3}) has a unitary cell formed of two identical cavities centered on the center of symmetry.[5] To model the polymer, an atomistic model previously used to calculate self-diffusion of gases in this crystal[12] was employed. In this model, the coordinates for the starting structure were taken from the experimental X-ray structure.[5] a, b, and c axes were matched with Cartesian x, y, and z axis, and a periodic system of 2 cells stacked in the a direction, 3 along b, and 4 in the c direction was considered. The resulting super cell is formed of 3072 atoms in an almost cubic simulation box of dimensions of L_x = 3.50 nm, L_y = 3.54 nm, and L_z = 3.12 nm. The all-atom force field nonbonded interactions (Lennard-Jones, Coulombic, and reaction field) and bonded interaction (bending and torsion) details can be found elsewhere.[13] The polymer system was equilibrated

Table 1. Nonbonded Parameters Taken from Ref 16. The Model Chosen for H H Interactions in Pure Hydrogen is the one Reported by Boanich in Ref 17

	σ /nm	ε/kJ mol^{-1}	q/e
pure components			
H (H_2)	0.2683	0.0936	+0.4432
center-of-mass H_2			−0.8864
atom−atom distance			
H_2 0.07508 nm			
C aliphatic	0.328	0.299	0
H aliphatic	0.258	0.189	0
C aromatic	0.355	0.294	−0.115
H aromatic	0.242	0.126	+0.115
cross-interactions			
C aliphatic-H (H_2)	0.298	0.2082	
H aliphatic-H (H_2)	0.263	0.1655	
C aromatic-H (H_2)	0.312	0.1659	
H aromatic-H (H_2)	0.255	0.1086	

by molecular dynamics (MD) at 77 K; the details for this procedure can be found in ref 12.

***ε* Crystalline Phase.** The orthorhombic structure of the ε polymorph of s-PS (a = 1.62 nm, b = 2.20 nm, c = 0.79 nm) has four chains per unit cell, a minimum center-to-center distance between channels of 1.36 nm, and a density close to 0.98 g cm^{-3}. To model this crystal, we used the coordinates of the unitary cell fitted to the X-ray characterization performed by Petraccone et al.,[6] and then we repeated it 3 times in the x direction, 2 in the y, and 4 in the z to produce a supercell of 6144 atoms and with initial box lengths of L_x = 4.86 nm, L_y = 4.4 nm, and L_z = 3.16 nm. The all-atom force field used was the same used for the δ phase. Molecular dynamics simulations using the GROMACS simulation package[14] were performed to relax the structure at 77 K and 0.1 MPa during 4 ns with time step equal to 0.002 ps. In the simulations the pressure P and the temperature T were kept constant using the Berendsen manostat and thermostat, respectively, with coupling times (P and T) of 0.5 ps. All bonds were kept rigid by means of LINCS constraint algorithm. The cutoff radius for nonbonded contributions was of 1.0 nm with a twin cutoff approach for neighbor list (cutoff = 1.0 nm and updated every 15 time steps), and full periodic boundary conditions were applied. The dielectric constant for the reaction field contribution was fixed at 2.5 (experimental value for amorphous polystyrene: 2.55 at 298.15 K[15]).

Hydrogen Model. The hydrogen was modeled as a two-center Lennard-Jones fluid with the addition of Coulombic charges placed on hydrogen sites (positive part) and on molecular center of mass (negative part) to represent the electric quadrupole moment of the molecule. In particular, the model has been derived by some of the authors using ab initio techniques and molecular dynamic simulations specifically for interaction of molecular hydrogen with polymers containing aromatic and aliphatic carbons. Parameters for those specific interactions (hydrogen−aliphatic and hydrogen−aromatic systems) were considered avoiding the simple use of Lorentz−Berthelot combining rules and were optimized on the basis of a correct reproduction of experimental data of hydrogen solubility in liquid benzene and cyclohexane, calculated using the test particle insertion method.[16] These parameters are shown in Table 1. The cutoff radius used was the half of the box for all the interactions, and long-range corrections were applied in the calculation of the configurational energy for the Lennard-Jones fluid−fluid interactions, assuming that the radial distribution functions are unity beyond the cutoff radius. The Coulombic contribution was treated using the reaction field method[18] with the dielectric constant of 2.5 for the hydrogen−hydrogen interactions (because every hydrogen molecule is surrounded mainly by polymer atoms).

Cross-Interactions. For the cross-parameters (to calculate the interaction between the adsorbent and the adsorbate) we used the parameters recently proposed to treat interactions in aliphatic and aromatic hydrocarbons, and they are summarized in Table 1. Because the polymer is composed mainly for these two types of interactions, we expect to have better predictions using these parameters instead of simply using a mixing rule. Lennard-Jones long-range corrections were included in the calculation of the cross-interactions, and reaction field (dielectric constant of 2.5) correction to the Coulombic term was also applied.

GCMC Simulation Details. The total potential energy between a fluid molecule and the polymer was calculated as the sum of the contributions of all the substrate atoms. The total energy for the system is the sum of this contribution over all the hydrogen molecules plus the sum of all fluid−fluid interactions. In the model used there are not interactions among the atoms of the polymer after the original equilibration by molecular dynamics. This assumption is valid, even when the pressure of bulk hydrogen goes to its higher values because the temperature is low, and then the polymer structure does not have a meaningful change.

In GCMC simulations, the temperature, the volume, and the chemical potential of the fluid inside the substrate are thus fixed. To consider the effect of the pressure, simulations at different value of chemical potential were run. To relate the chemical potential with the corresponding values of pressure in the bulk phase, we performed GCMC simulations in the bulk phase at the values of chemical potential of interest. Three different types of Monte Carlo trials were considered in the simulations: creation of a new adsorbate molecule at a random position inside the adsorbent material, removal of a randomly chosen hydrogen, and move of a randomly chosen fluid particle (both translation and rotation moves). The simulations were performed by cycles, and each cycle consisted of different types of attempted MC moves: N displacement moves (translation and rotation equally probable) and $100N$ creation/destruction of a particle (again, chosen with equal probability), where N is proportional to the number of molecules of hydrogen. After an initial equilibration period of $\approx 6 \times 10^4$ cycles, typically 1×10^5 cycles were generated to accumulate the averages of the desired quantities. The precisions of the simulated results were obtained using block averages with 1000 cycles per block.

We treated hydrogen as a classical fluid, and therefore, we did not apply quantum corrections. At 77 K and at the intermediate and higher pressures used in this work, the quantum effect is non-negligible.[19] But because we are comparing results calculated in the same way, in systems of approximated the same size, we expect that this effect contributes more or less equally in both cases. It is worth adding that the parameters used to model the hydrogen very well reproduce the bulk behavior of molecular hydrogen because (as discussed above) the comparison between experiments[20] and simulations[16] is very good.

Results and Discussion

Experimental Studies. The H_2 sorption from s-PS films (thickness in the range 10−30 μm) at 77 K is negligible, independently of the nature of their crystalline phase.

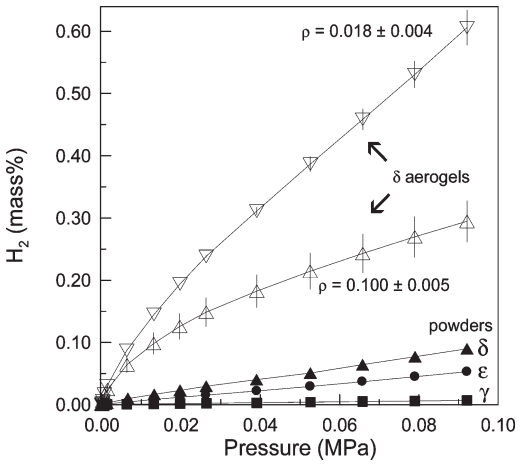

Figure 1. H_2 gravimetric adsorption isotherms, for pressure lower than 0.1 MPa at 77 K, on s-PS powders exhibiting the nanoporous δ (▲), the nanoporous ε (●), and the dense γ (■) crystalline phases and for s-PS aerogels exhibiting the nanoporous δ phase and different apparent densities (△, $\rho = 0.100 \pm 0.005$ g/cm^3; ▽, $\rho = 0.018 \pm 0.004$ g/cm^3).

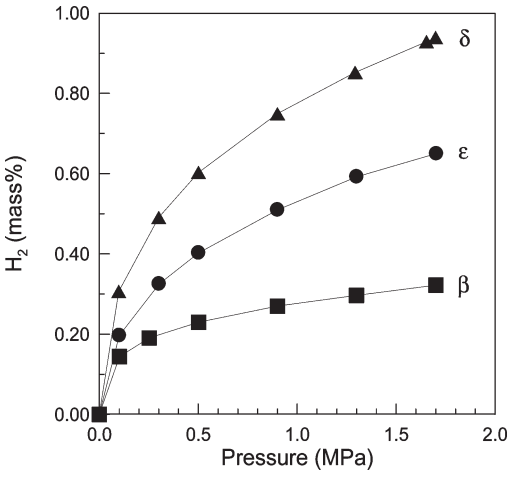

Figure 2. H_2 gravimetric adsorption isotherms recorded at 77 K on s-PS aerogels, with similar crystallinity, morphology, and porosity, exhibiting the nanoporous δ (▲), nanoporous ε (●), and the dense β (■) crystalline phases.

The H_2 sorption isotherms recorded at 77 K for a same s-PS powder, after subsequent crystal-to crystal transitions ($\gamma \rightarrow \delta \rightarrow \gamma \rightarrow \varepsilon$),[6b] exhibiting the nanoporous δ and ε or the dense γ crystalline phases are shown as filled symbols in Figure 1. Although the hydrogen sorption remains low, a clear increase of the sorption for the powders presenting the nanoporous crystalline phases occurs. In particular, for the δ form powder there is a sorption increase of nearly 1 order of magnitude with respect to the γ form powder.

The H_2 sorption isotherms recorded at 77 K for s-PS aerogels exhibiting the nanoporous δ phase and different apparent densities are also shown in Figure 1. It is immediately apparent that the sorption capacity of the δ form samples can be largely increased by using s-PS aerogels, i.e., samples presenting more open morphologies, and that the sorption capacity is particularly high for the aerogel presenting the highest porosity (nearly 98%) and hence a very low apparent density ($\rho \approx 0.02$ g/cm^3).

H_2 sorption isotherms have been also measured in a wider pressure range (up to 1.7 MPa) on aerogels exhibiting the two nanoporous (δ and ε) and the dense β crystalline phases, with similar degree of crystallinity (35−40%), porosity ($88\% < P < 95\%$ corresponding to apparent densities in the range 0.045 g/cm^3 $< \rho <$ 0.120 g/cm^3), and similar nanofibrillar morphology (Figure 2).

It is clearly shown that, for the entire H_2 pressure range, the H_2 uptake is minimum for the β aerogels, i.e., aerogels with a dense crystalline phase, while it is definitely higher for ε and δ aerogels, i.e., aerogels with nanoporous crystalline phases.

As for the gravimetric isotherms of Figure 2, it is worth adding that for the β aerogels, which absorb hydrogen molecules only in the amorphous phase,[3] the observed behavior can be described in terms of the dual-mode sorption model:[21] i.e., Langmuir sorption in the microvoid regions dominates at low gas pressures while Henry sorption in the polymer matrix component dominates at high pressures. Of course, for the δ and ε aerogels the interpretation of the sorption phenomena is further complicated by the occurrence of additional gas sorption in the crystalline microvoids.

To better understand the largely different H_2 uptakes from aerogels presenting similar porosities and different crystalline phases, the FTIR spectra of H_2 adsorbed at 20 K on the β-, ε-, and δ-aerogels have been reported in Figure 3. As outlined in the Experimental Section, the spectral series of Figure 3 were recorded by progressively *decreasing* the H_2 equilibrium pressure at 20 K. Nevertheless, to allow better comparison of the IR data with the molecular simulations (vide infra), they will be discussed here as obtained by the opposite procedure, i.e., upon *increasing* the H_2 pressure. This is fully justified by the reversible nature of the adsorption process.

On the basis of Figure 3, the following can be noted: (i) In the spectra of H_2 adsorbed on the ε and δ phases a couple of bands is formed already at low pressure at 4117 and 4107 cm^{-1} (i.e., ca. 40−50 cm^{-1} lower than the Raman frequency of gaseous H_2). The 4117−4107 cm^{-1} doublet rapidly reaches the maximum intensity by further H_2 dosage. Upon further increase of the H_2 equilibrium pressure, new and more intense absorptions gradually develop in the 4160−4120 cm^{-1} region of the spectra. (ii) In agreement with the gravimetric results of Figures 1 and 2, the intensities of these H_2 bands are weak, intermediate, and strong in the spectra of β-, ε-, and δ-aerogels, respectively. (iii) The spectra observed for ε- and δ-aerogels show not only an overall similarity but also similar absorption frequencies. This indicates that the observed bands are due to H_2 adducts involving adsorption sites that are structurally (and energetically) similar for the two crystalline phases.

These observations support the previous hypothesis[3] that the narrow bands of the spectra of H_2 adsorbed on s-PS aerogels are due to hydrogen molecules encapsulated inside the nanoporous crystalline phases of the aerogels. Of course, in this framework, the lower H_2 sorption by the aerogels exhibiting the dense β (or γ) phase would be due to the adsorption on the nanofibril surfaces.

Further comments relative to these FTIR spectra will be added on the basis of a comparison with the molecular simulation results of the next section.

It is also worth adding that the uptake from s-PS samples of guest molecules (like, e.g., aromatic and/or chlorinated volatile organic compounds, presenting a good solubility in both their amorphous and nanoporous crystalline phases) depends on the kind (δ or ε) and degree of crystallinity of the nanoporous crystalline phase while is generally independent of the sample morphology. Just as an example, the 1,2-dichloroethane uptake from 10 ppm water solution is nearly 5 wt % for both low-density aerogels and thick films.[9c]

The uptake behavior presently described for molecular hydrogen (Figures 1−3) is completely different. In fact, it is

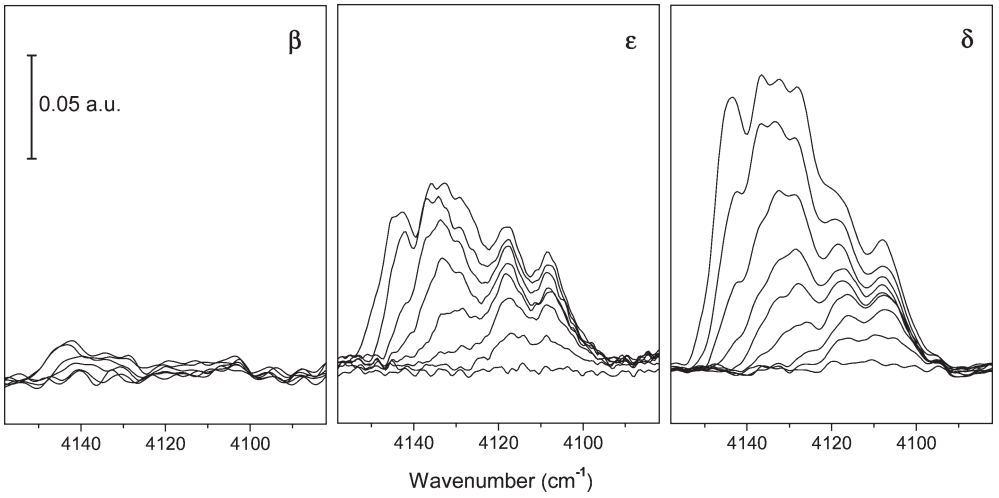

Figure 3. FTIR spectra of increasing doses of H_2 adsorbed at 20 K on s-PS aerogels exhibiting the β, ε, and δ crystalline phases. In all cases the H_2 equilibrium pressure varied between 0 (less intense spectrum) and ca. 0.2 kPa (most intense spectrum).

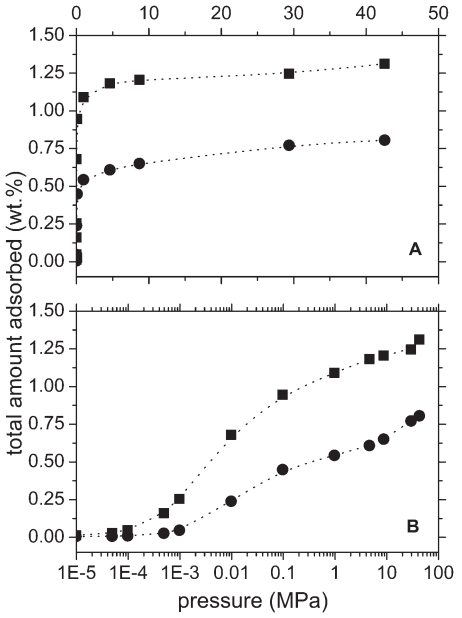

Figure 4. Gravimetric sorption isotherms of H_2 in δ (squares) and in ε (circles) s-PS at 77 K by GCMC simulations. The data are presented in two different scales of the pressure axis (A, linear; and B, logarithmic). The dotted lines are guides for the eyes.

negligible for films and poor for powders while for aerogels progressively increases by reducing their density (and hence increasing their surface area). It is reasonable to assume that in dense samples (film and powders) the H_2 uptake from the nanoporous crystalline phases is limited by the poor H_2 solubility in the amorphous phase (having a density, 1.05 g/cm^3, definitely higher than for the nanoporous crystalline phases, 0.98 g/cm^3).[22] In this framework, the much higher uptake from the aerogels would be due to the easier accessibility of the nanoporous crystalline phase.

Molecular Simulations. Figure 4 shows the total gravimetric amount of hydrogen adsorbed by both nanoporous polymorphs of s-PS (δ and ε), at 77 K as a function of pressure, calculated by GCMC simulations. For the sake of clarity, the plot is presented also in logarithmic scale (Figure 4B), and dotted lines are added as eye guides.

In the lower range of pressures ($P_{H_2} < 0.001$ MPa), the adsorption calculated for the δ form is nearly 4−5 times higher than for the ε form. Increasing the pressure, the adsorption from both nanoporous crystalline phases increases and the ratio between the calculated adsorptions for the δ and ε forms is reduced to 1.6.

The higher hydrogen sorption capacity of the δ form with respect to the ε form is due to the different spatial distribution of the same amount of empty space of the crystalline phases (both having a density of 0.98 g/cm^3), i.e., to the higher potential exerted by the walls, where the pronounced curvature of the cavities produces an overlapped potential.

The packing models of the δ and ε crystalline forms of s-PS in two different projections (along the *c* (A) and *a* (B) axes) are shown in the upper parts of Figures 5 and 6, respectively. Snapshots taken from the simulations at 0.01 and 30 MPa for both forms are shown in the central (C, D) and lower part (E, F) of the same figures.

As for the δ form, the obtained results (Figure 5) indicate that, for both low- and high-pressure simulations, the hydrogen molecules are absorbed into the crystalline cavities (Figure 5A), which are essentially confined by eight phenyl rings of adjacent enantiomorphous helices. Moreover, at low pressure, the H_2 molecules tend to preferentially occupy intrachain locations, i.e., to be close to the two chains that confine the cavity. This is, e.g., shown by the along *a* view of Figure 5D, exhibiting an essentially empty central part of the cavities. On the other hand, for high pressures, up to four H_2 molecules can be clustered for each cavity (see Figure 5E).

As for the ε form, the obtained results (Figure 6) indicate that, for both low- and high-pressure simulations, the hydrogen molecules are absorbed only into the channels, preferentially in their central part (Figure 6D,F).

On the basis of these considerations, we have replotted the calculated data of Figure 4A by indicating by dashed straight lines the weight amount of H_2 corresponding to a given number of molecules per cavity and per unit height for the δ (Figure 7A) and ε (Figure 7B) crystalline forms, respectively.

It is clearly apparent that the calculated plateau values, as achieved for high hydrogen pressures, correspond to average contents of nearly 3 molecules per cavity and of 3.5 molecules per unit height for the δ and ε phases, respectively.

The calculated distribution of the H_2 molecules in the cavities of δ form of s-PS has been examined for different pressures by taking averages over all the equilibrated configurations. In particular, the H_2 distribution in the crystalline cavities of the δ form, as calculated at 77 K for five different pressure values in the range 0.001−2.1 MPa, are reported in Figure 8.

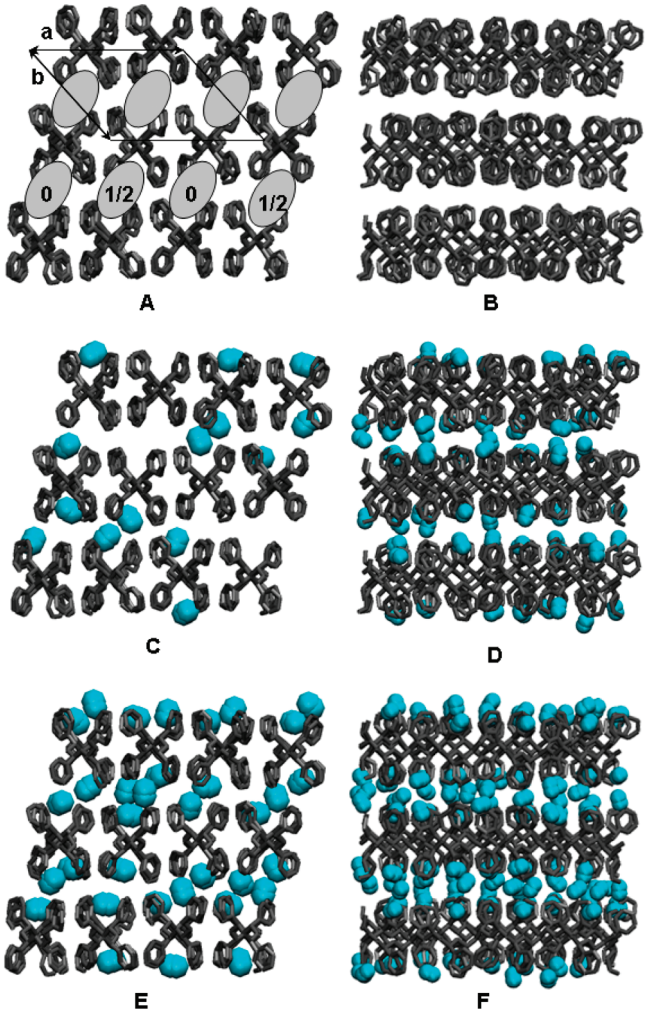

Figure 5. Snapshots of adsorbed hydrogen on δ s-PS at 77 K by GCMC simulations, as projected along the *c* axis (A, C, E) or along the *a* axis (B, D, F). The gray bonds represent the polymer structure (just C atoms), and the cyan spheres are the molecules of hydrogen. Simulations ran at 0.01 MPa (C, D) and at 30 MPa (E, F). The unit cell of the δ phase and the relative height of adjacent cavities are shown in (A). For the sake of clarity, for the top views (C, E), only hydrogen molecules absorbed in a layer having a thickness equal to the unit height of the crystalline form (0.78 nm) are shown.

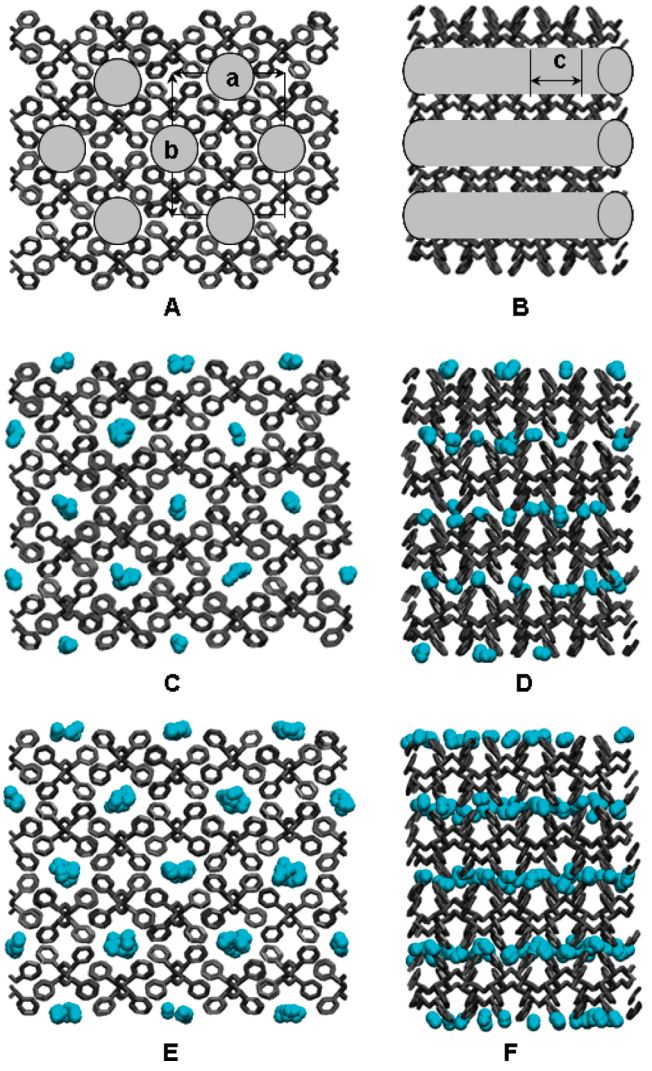

Figure 6. Snapshots of adsorbed hydrogen on ε s-PS at 77 K by GCMC simulations, as projected along the *c* axis (A, C, E) or along the *a* axis (B, D, F). The gray bonds represent the polymer structure (just C atoms), and the cyan spheres are the molecules of hydrogen. Simulations ran at 0.01 MPa (C, D) and at 30 MPa (E, F). The unit cell of the ε phase is shown in (A), together with circles schematically indicating the channels projections.

The results relative to the low H_2 pressure (see, e.g., P_{H_2} = 0.0014 MPa) clearly indicate that there is neither attraction nor repulsion between hydrogen molecules into the cavities of the δ crystalline form. In fact, the amount of cavities without H_2 molecules is similar to the amount of cavities with 2 H_2 molecules. On the other hand, the results at high H_2 pressure clearly indicate that the addition in a cavity already occupied by 3 molecules of a fourth H_2 molecule involves some relevant steric repulsion. In fact, for instance, for the distribution calculated at P_{H_2} = 2.1 MPa, although the maximum probability is associated with 3 molecules per cavity, the amount of cavities filled by 4 H_2 molecules is much smaller than the amount of cavities filled by 2 H_2 molecules.

We have also evaluated the possible occurrence of some average orientation of the hydrogen molecules inside the cavities or the channels of the nanoporous crystalline phases. In particular, we calculated the angle between the bond axis of H_2 and the chain axes of the polymer and the related order parameter. The results averaged over all the equilibrated configurations (and along the adsorption isotherms) showed that the orientation is mainly random; i.e., contrary to the case of most s-PS guest molecules[23] (also being gases like ethylene[24] and carbon dioxide[25]), there is not a significant molecular hydrogen orientation, for both nanoporous phases.

Considerations Based on Both Experiments and Simulations. The plot of Figure 9A compares the sorption isotherms for the two nanoporous crystalline phases, as calculated by GCMC simulations (dotted lines, taken from Figure 4A) and as obtained from the experimental data for semicrystalline samples (continuous lines). In particular, it is assumed that the overall adsorption by the macropores of the amorphous phase (i.e., by the surface of the nanofibrils) is equal to the overal sorption of the β aerogel, having similar degrees of crystallinity, porosity, and morphology, in the same sorption conditions ($S_{exp\beta}$, see, e.g., squares in Figure 2). Hence, the sorption by the δ and ε crystalline phases of the aerogels ($S_{crys\delta}$ and $S_{crys\,\varepsilon}$, respectively) have been derived as

$$S_{crys}\delta = (S_{exp}\delta - S_{exp}\beta)/x_\delta$$

$$S_{crys}\varepsilon = (S_{exp}\varepsilon - S_{exp}\beta)/x_\varepsilon$$

where x_δ and x_ε are the degrees of crystallinity of the δ and ε aerogels.

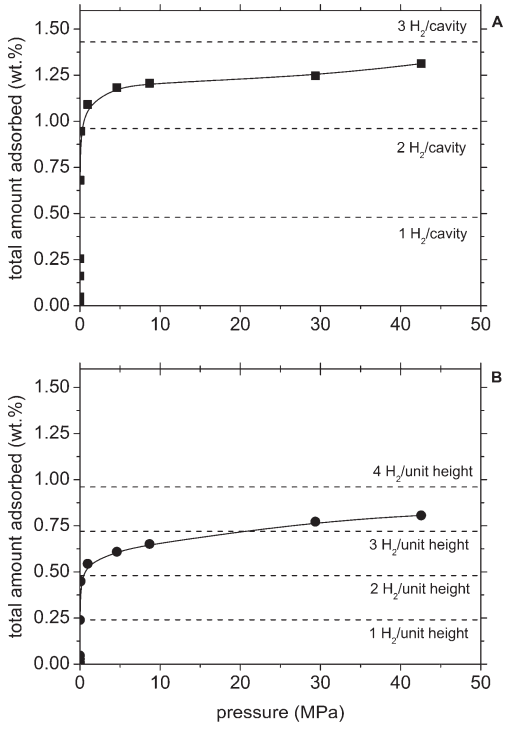

Figure 7. Gravimetric sorption isotherms of H_2 in δ (A) and in ε (B) s-PS at 77 K, as calculated by GCMC simulations. The horizontal lines indicate the weight increase corresponding to the uptake of a given number of hydrogen molecules per cavity of the δ form or per unit height for the ε form.

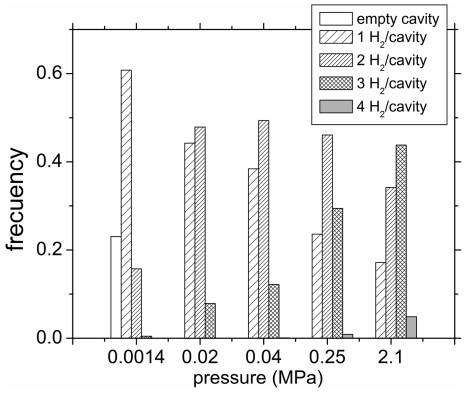

Figure 8. Distribution of the number of H_2 molecules per cavity of the δ phase of s-PS as calculated from GCMC simulations at 77 K and at different H_2 pressures.

The plot of Figure 9B compares the same sorption isotherms of Figure 9A, but reporting the gravimetric excess adsorption with respect to hydrogen in bulk phase at the same state conditions (temperature and pressure).

The plots of Figure 9 show that the calculated and the experimental H_2 uptakes are similar. In particular, for both experiments and simulations, although the two nanoporous crystalline phases present essentially the same density, the uptake from the δ phase is nearly double with respect to the uptake from the ε phase. The occurrence of larger experimental uptakes, for high pressures, is possibly due to the rigidity of the polymer host structure assumed in our molecular simulations. This comparison between experimental and calculated uptakes also suggests that for aerogels with porosity higher than 90% most of the crystalline pores become accessible, provided that a sufficient H_2 pressure is

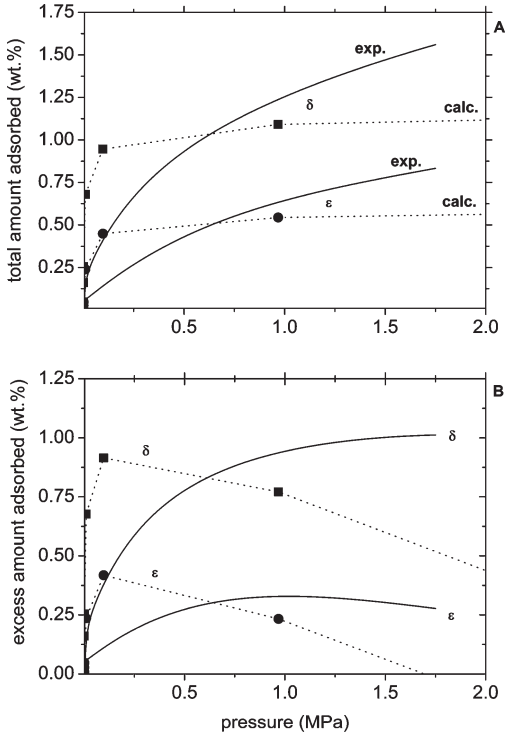

Figure 9. Gravimetric (A) and excess gravimetric adsorption (B) isotherms of H_2 in δ (squares) and in ε (circles) s-PS crystalline phases at 77 K. The continuous lines have been obtained by the experimental data of Figure 2, after subtraction of the adsorption from the microfibril surfaces (assumed equal to the adsorption of the analogous β-form aerogel). The dotted lines correspond to the data calculated by the GCMC simulations of Figure 4.

reached. In particular, for both δ and ε aerogels the gravimetric excess adsorption reaches its maximum already for H_2 pressure not far from 1.5 MPa.

Molecular simulation results like those of Figure 8 can contribute to rationalize the FTIR spectra of H_2 adsorbed on s-PS aerogels, like those of Figure 3. In fact, the molecular simulations indicate that at low pressures only one or two H_2 molecules are adsorbed per cavity of the δ crystalline phase. It is therefore conceivable that the 4117−4107 cm^{-1} bands represent the spectroscopic fingerprint of isolated or couples of H_2 included in the crystalline cavities. According to the molecular simulations, at higher pressures, clusters $(H_2)_n$ with $n = 3$ or 4, implying some intermolecular steric repulsion, become feasible. These clusters could produce the more intense bands in the 4160−4120 cm^{-1} region of the spectra.

Conclusions

The H_2 uptake from s-PS samples exhibiting different crystalline phases and different morphologies has been studied by gravimetric measurements at 77 K, in the hydrogen pressure range from 0 up to 1.7 MPa, and compared with molecular simulations relative to s-PS crystals.

Gravimetric experiments show that the molecular hydrogen sorption is strongly dependent on the sample morphology, i.e., negligible for films, poor for powders, higher and increasing with porosity for aerogels. This clearly indicates that, as usual for carbon-based adsorbents, the H_2 uptake increases with the sample surface area.

However, for a given morphology (for both powders and aerogels), the H_2 uptake is also strongly dependent on the nature of the crystalline phase. In particular, the H_2 uptake is minimum for the dense β and γ crystalline phases, intermediate for the

channel-shaped nanoporous ε phase and highest for the cavity-shaped nanoporous δ phase. A comparison between H_2 uptake from aerogels exhibiting similar porosity, morphology, and degree of crystallinity, but different crystalline phases, indicates that the absorption by the crystalline cavities of the δ phase is much higher than the surface adsorption.

The occurrence of molecular hydrogen absorption in the crystalline cavities is clearly confirmed by FTIR spectra, as collected at 20 K, showing narrow components of the H_2 band for aerogels exhibiting both nanoporous (δ and ε) crystalline phases and only broad and very weak signals for aerogels exhibiting dense s-PS crystalline phases.

The reported GCMC simulations clearly indicate that, for both low and high pressure, the hydrogen molecules are absorbed into the crystalline cavities and channels of the δ and ε crystalline phases, respectively. In particular, large uptakes are already reached for low H_2 pressures, and limit sorption values correspond to average contents of nearly 3 molecules per cavity and of 3.5 molecules per unit height for the δ and ε phases, respectively. The distribution of the H_2 molecules in the cavities of δ form of s-PS also indicates that there is neither attraction nor repulsion between hydrogen molecules into the cavities, while the addition in a cavity already occupied by 3 molecules of a fourth H_2 molecule involves some relevant steric repulsion.

The agreement between experimental and calculated H_2 sorption for both nanoporous crystalline phases is satisfactory. In fact, although the two nanoporous crystalline phases present essentially the same density (0.98 g/cm^3), for both experiments and simulations, the uptake from the δ phase is roughly double with respect to the uptake from the ε phase.

Hence, the present study indicates that nanoporous materials with low density crystalline phases and small crystalline cavities can be suitable for H_2 uptake. To further increase the H_2 uptake from carbon-based materials, low-density crystalline phases with crystalline cavities smaller than those of the δ phase ($\approx$ 0.12 nm^3)[5b] would be needed.

It is also worth adding that, although the H_2 uptake from the polymeric nanoporous crystalline phases is similar to those of other adsorbing materials like, e.g., porous carbons, nanotubes, zeolites, porous polymers, and metal−organic frameworks,[1] it is definitely lower than needed for industrially useful H_2 storage applications. The novelty with respect to other carbonaceous materials described in the literature is the coexistence of two additive sorption phenomena, occurring at the surface of the amorphous phase (as found on conventional amorphous carbon surfaces) and a second on the crystalline phase.

Acknowledgment. Financial support of the "Ministero dell'Istruzione, dell'Università e della Ricerca" (PRIN07), of "Regione Campania" (Legge 5 and Centro di Competenza per le Attività Produttive), and of "Regione Piemonte" ("Progetto Regionale Materiali Innovativi per lo Stoccaggio di Idrogeno") is acknowledged. We thank Prof. Adriano Zecchina of the University of Turin and Prof. Luigi Cavallo and Prof. Vincenzo Venditto of the University of Salerno for useful discussions.

References and Notes

(1) (a) Felderhoff, M.; Weidenthaler, C.; von Helmolt, R.; Eberle, U. *Phys. Chem. Chem. Phys.* **2007**, *9*, 2643. (b) Van den Berg, A. W. C.; Otero Areán, C. *Chem. Commun.* **2008**, 668.
(2) Germain, J.; Fréchet, J. M. J.; Svec, F. *Small* **2009**, *5*, 1098.
(3) Figueroa-Gerstenmaier, S.; Daniel, C.; Milano, G.; Guerra, G.; Zavorotynska, O.; Vitillo, J. G.; Zecchina, A.; Spoto, G. *Phys. Chem. Chem. Phys.* **2010**, *12*, 5369.
(4) (a) Milano, G.; Guerra, G. *Prog. Mater. Sci.* **2009**, *54*, 68. (b) Albunia, A. R.; D'Aniello, C.; Guerra, G. In Schellenberg, J., Ed.; *Syndiotactic Polystyrene: Synthesis, Characterization, Processing and Applications*; Wiley: New York, 2010; Chapter 10.
(5) (a) De Rosa, C.; Guerra, G.; Petraccone, V.; Pirozzi, B. *Macromolecules* **1997**, *30*, 4147. (b) Milano, G.; Venditto, V.; Guerra, G.; Cavallo, L.; Ciambelli, P.; Sannino, D. *Chem. Mater.* **2001**, *13*, 1506.
(6) (a) Petraccone, V.; Ruiz de Ballesteros, O.; Tarallo, O.; Rizzo, P.; Guerra, G. *Chem. Mater.* **2008**, *20*, 3663. (b) Rizzo, P.; D'Aniello, C.; De Girolamo Del Mauro, A.; Guerra, G. *Macromolecules* **2007**, *40*, 9470. (c) Tarallo, O.; Schiavone, M. M.; Petraccone, V.; Daniel, C.; Rizzo, P.; Guerra, G. *Macromolecules* **2010**, *43*, 1455.
(7) (a) Manfredi, C.; Del Nobile, M. A.; Mensitieri, G.; Guerra, G.; Rapacciuolo, M. *J. Polym. Sci., Polym. Phys. Ed.* **1997**, *35*, 133. (b) Guerra, G.; Manfredi, C.; Musto, P.; Tavone, S. *Macromolecules* **1998**, *31*, 1329. (c) Musto, P.; Mensitieri, G.; Cotugno, S.; Guerra, G.; Venditto, V. *Macromolecules* **2002**, *35*, 2296. (d) Mahesh, K. P. O.; Sivakumar, M.; Yamamoto, Y.; Tsujita, Y.; Yoshimizu, H.; Okamoto, S. *J. Membr. Sci.* **2005**, *262*, 11. (e) Mensitieri, G.; Larobina, D.; Guerra, G.; Venditto, V.; Fermeglia, M.; Pricl, S. *J. Polym. Sci., Part B: Polym. Phys.* **2008**, *46*, 8.
(8) (a) Chatani, Y.; Inagaki, T.; Shimane, Y.; Ijitsu, T.; Yukimori, T.; Shikuma, H. *Polymer* **1993**, *34*, 1620. (b) Chatani, Y.; Shimane, Y.; Inagaki, T.; Shikuma, H. *Polymer* **1993**, *34*, 4841. (c) De Rosa, C.; Rizzo, P.; Ruiz de Ballesteros, O.; Petraccone, V.; Guerra, G. *Polymer* **1999**, *40*, 2103. (d) Tarallo, O.; Petraccone, V. *Macromol. Chem. Phys.* **2004**, *205*, 1351. (e) Petraccone, V.; Tarallo, O.; Venditto, V.; Guerra, G. *Macromolecules* **2005**, *38*, 6965. (f) Tarallo, O.; Petraccone, V.; Venditto, V.; Guerra, G. *Polymer* **2006**, *47*, 2402. (g) Tarallo, O.; Petraccone, V.; Daniel, C.; Guerra, G. *Cryst. Eng. Commun.* **2009**, *11*, 2381.
(9) (a) Daniel, C.; Alfano, D.; Venditto, V.; Cardea, S.; Reverchon, E.; Larobina, D.; Mensitieri, G.; Guerra, G. *Adv. Mater.* **2005**, *17*, 1515. (b) Malik, S.; Roizard, D.; Guenet, J. M. *Macromolecules* **2006**, *39*, 5957. (c) Daniel, C.; Sannino, D.; Guerra, G. *Chem. Mater.* **2008**, *20*, 577. (d) Daniel, C.; Giudice, S.; Guerra, G. *Chem. Mater.* **2009**, *21*, 1028.
(10) (a) De Rosa, C.; Rapacciuolo, M.; Guerra, G.; Petraccone, V.; Corradini, P. *Polymer* **1992**, *33*, 1423. (b) Chatani, Y.; Shimane, Y.; Ijitsu, T.; Yukinari, T. *Polymer* **1993**, *34*, 1625.
(11) (a) Immirzi, A.; de Candia, F.; Iannelli, P.; Zambelli, A.; Vittoria, V. *Makromol. Chem., Rapid Commun.* **1988**, *9*, 761. (b) Rizzo, P.; Lamberti, M.; Albunia, A. R.; Ruiz de Ballesteros, O.; Guerra, G. *Macromolecules* **2002**, *35*, 5854. (c) Tamai, Y.; Fukuda, M. *Macromol. Rapid Commun.* **2002**, *23*, 892. (d) Rizzo, P.; Albunia, A. R.; Guerra, G. *Polymer* **2005**, *46*, 9549.
(12) Milano, G.; Guerra, G.; Müller-Plathe, F. *Chem. Mater.* **2002**, *14*, 2977.
(13) Müller-Plathe, F. *Macromolecules* **1996**, *29*, 4782.
(14) (a) Lindahl, E.; Hess, B.; van der Spoel, D. *J. Mol. Model.* **2001**, *7*, 306. (b) Berendsen, H. J.C.; van der Spoel, D.; van Drunen, R. *Comput. Phys. Commun.* **1995**, *91*, 43.
(15) Lide, D. R., Ed.; *CRC Handbook of Chemistry and Physics*, 75th ed.; CRC Press: Boca Raton, FL, 1994−95.
(16) Figueroa-Gerstenmaier, S.; Giudice, S.; Cavallo, L.; Milano, G. *Phys. Chem. Chem. Phys.* **2009**, *11*, 3935.
(17) Bouanich, J.-P. *J. Quant. Spectrosc. Radiat. Transfer* **1992**, *47*, 243.
(18) Jedlovszky, P.; Pálinkás, G. *Mol. Phys.* **1995**, *84*, 217.
(19) Kowalczyk, P.; Tanaka, H.; Holyst, R.; Kaneko, K.; Ohmori, T.; Miyamoto, J. *J. Phys. Chem. B* **2005**, *109*, 17174.
(20) NIST Standard Reference Database 69, June 2005 Release: NIST Chemistry WebBook.
(21) (a) Hofmann, D.; Ulbrich, J.; Fritsch, D.; Paul, D. *Polymer* **1996**, *37*, 4773. (b) Tsujita, Y. *Prog. Polym. Sci.* **2003**, *28*, 1377.
(22) (a) Manfredi, C.; De Rosa, C.; Guerra, G.; Rapacciuolo, M.; Auriemma, F.; Corradini, P. *Macromol. Chem. Phys.* **1995**, *196*, 2795. (b) Larobina, D.; Sanguigno, L.; Venditto, V.; Guerra, G.; Mensitieri, G. *Polymer* **2004**, *45*, 429.
(23) (a) Albunia, A. R.; Di Masi, S.; Rizzo, P.; Milano, G.; Musto, P.; Guerra, G. *Macromolecules* **2003**, *36*, 8695. (b) Albunia, A. R.; Milano, G.; Venditto, V.; Guerra, G. *J. Am. Chem. Soc.* **2005**, *127*, 13114. (c) Itagaki, H.; Sago, T.; Uematsu, M.; Yoshioka, G.; Correa, A.; Venditto, V.; Guerra, G. *Macromolecules* **2008**, *41*, 9156.
(24) Albunia, A. R.; Minucci, T.; Guerra, G. *J. Mater. Chem.* **2008**, *18*, 1046.
(25) Annunziata, L.; Albunia, A. R.; Venditto, V.; Guerra, G. *Macromolecules* **2006**, *39*, 9166.